Effects of Horizontal Diffusion on Tropical Cyclone Intensity Change and Structure in Idealized Three-Dimensional Numerical Simulations

JUN A. ZHANG

NOAA/AOML/Hurricane Research Division, and Cooperative Institute for Marine and Atmospheric Studies, University of Miami, Miami, Florida

FRANK D. MARKS

NOAA/AOML/Hurricane Research Division, Miami, Florida

(Manuscript received 15 October 2014, in final form 17 July 2015)

ABSTRACT

This study examines the effects of horizontal diffusion on tropical cyclone (TC) intensity change and structure using idealized simulations of the Hurricane Weather Research and Forecasting Model (HWRF). A series of sensitivity experiments were conducted with varying horizontal mixing lengths (L_h), but kept the vertical diffusion coefficient and other physical parameterizations unchanged. The results show that both simulated maximum intensity and intensity change are sensitive to the L_h used in the parameterization of the horizontal turbulent flux, in particular, for L_h less than the model's horizontal resolution. The results also show that simulated storm structures such as storm size, kinematic boundary layer height, and eyewall slope are sensitive to L_h as well. However, L_h has little impact on the magnitude of the surface inflow angle and thermodynamic mixed layer height. Angular momentum budget analyses indicate that the effect of L_h is to mainly spin down a TC vortex. Both mean and eddy advection terms in the angular momentum budget are affected by the magnitude of L_h. For smaller L_h, the convergence of angular momentum is larger in the boundary layer, which leads to a faster spinup of the vortex. The resolved eddy advection of angular momentum plays an important role in the spinup of the low-level vortex inward from the radius of the maximum wind speed when L_h is small.

1. Introduction

The maintenance and intensification of a tropical cyclone (TC) is strongly tied to turbulent transport processes, in particular, turbulence in the boundary layer and the eyewall region within and above the boundary layer (e.g., Emanuel 1995; Persing and Montgomery 2003; Rotunno et al. 2009; Smith et al. 2009; Bryan 2012). The importance of vertical mixing on TC intensity and structure, especially the boundary layer structure, has been extensively studied (Braun and Tao 2000; Kepert 2001; Kepert and Wang 2001; Foster 2009; Nolan et al. 2009a; Kepert 2010, 2012; Zhang et al. 2012; Gopalakrishnan et al. 2013; Zhu et al. 2014). Recently, horizontal diffusion has also been shown to be an important element in both theoretical and numerical simulations of TC intensification and the TC maximum potential intensity (MPI; Emanuel 1997; Bryan and Rotunno 2009, hereafter BR09; Bryan 2012; Rotunno and Bryan 2012, hereafter RB12). In particular, BR09 demonstrated that the maximum intensity of their simulated TCs was very sensitive to the horizontal mixing length in an axisymmetric numerical cloud model. Bryan et al. (2010) ran three-dimensional model simulations to study the impact of horizontal mixing on MPI and confirmed the findings of BR09. Bryan (2012) also studied the effect of the ratio of enthalpy exchange coefficient C_k and drag coefficient C_d on the simulated MPI. RB12 studied both the effects of horizontal and vertical mixing on simulated TC structure and MPI. They proposed physical and dynamical explanations for why horizontal mixing length affected a storm's maximum intensity.

Despite the importance of turbulent mixing, observational data are scarce in high-wind-speed regimes, and the quantitative value and variation with wind speed of

Corresponding author address: Dr. Jun Zhang, NOAA/AOML/Hurricane Research Division, CIMAS, University of Miami, 4301 Rickenbacker Causeway, Miami, FL 33149.
E-mail: jun.zhang@noaa.gov

DOI: 10.1175/MWR-D-14-00341.1

the vertical and horizontal eddy diffusivities remain poorly understood. Fast-response (>10 Hz), flight-level data do not exist below 1 km in the TC eyewall region, which makes it impossible to directly compute turbulent fluxes in the high-wind regime. Through their analysis of very limited 1-Hz flight-level wind data collected in Hurricanes Allen (1980) and Hugo (1989), Zhang et al. (2011a) estimated the vertical eddy diffusivity for momentum flux, stating that vertical eddy diffusivity tended to increase with wind speed at ~500 m. That study led to significant improvements in the boundary layer physics of the operational Hurricane Weather Research and Forecasting Model (HWRF) (Zhang et al. 2012; Gopalakrishnan et al. 2013). Reducing the vertical eddy diffusivity in HWRF, based on the observations of Zhang et al. (2011a), improved TC intensity and track forecasts (Tallapragada et al. 2014; Zhang et al. 2015).

The only observational study of horizontal mixing in TCs was performed by Zhang and Montgomery (2012, hereafter ZM12). Within the context of simple K theory, ZM12 analyzed data collected in Hurricanes Allen (1980), David (1986), and Hugo (1989) to estimate horizontal eddy diffusivity and corresponding mixing length. They found that the horizontal mixing length was, on average, ~750 m in the eyewall region with a mean wind speed of ~55 m s^{-1} at ~500-m altitude. Of note, ZM12 also found that horizontal mixing length was not significantly dependent on wind speed. Consistent with BR09, ZM12 demonstrated that horizontal mixing by turbulence in the eyewall was an important aspect of the dynamics of TCs that should not be neglected in TC models.

In this study, we examine the effects of horizontal diffusion on TC intensity and structure using three-dimensional numerical simulations of the HWRF. Our aim is to quantify the sensitivity of simulated TC intensity change and structure to the horizontal mixing length L_h, thereby providing useful guidance to the modeling community charged with improving TC intensity forecasts.

2. The HWRF configuration and experiment design

The operational HWRF system was originally developed at NOAA/National Weather Service (NWS)/National Centers for Environmental Prediction (NCEP) in 2007. As part of NOAA's Hurricane Forecast Improvement Project (HFIP; Gall et al. 2013), the latest version of HWRF has a 3-km horizontal resolution for its inner nest. This version of HWRF was jointly developed by the Environmental Prediction Center (EMC) of the NCEP/Hurricane Research Division of the Atlantic Oceanographic and Meteorological Laboratory and the Physical Sciences Division of the Earth System Research Laboratory and can be accessed at the Developmental Testbed Center at the National Center for Atmospheric Research.

We used the triply nested version of HWRF in an idealized framework (Gopalakrishnan et al. 2011, 2012, 2013; Bao et al. 2012). The parent domain of the model covers 50° × 50° and has a coarse horizontal resolution of 27 km. The two inner nests have two-way interactions with the parent domain, with horizontal resolutions of 9 and 3 km, and cover ~15° × 15° and ~5° × 5°, respectively. The model has 42 hybrid vertical levels with more than 10 levels below the 850-hPa level. It is initialized by solving the nonlinear balance equation in the pressure-based sigma coordinate system on an f plane centered at 15°N following Wang (1995). The initial axisymmetric cyclonic vortex has a maximum wind speed of 20 m s^{-1} and a radius of maximum wind speed of about 90 km embedded in a quiescent flow. For simplicity, the environmental temperature and humidity fields in all of the experiments are from Jordan's Caribbean sounding (Gray et al. 1975); the sea surface temperature was set to a constant of 302 K with no landmasses in the three domains.

The model physics options used in this study were configured as close as possible to the operational HWRF in a similar manner to Gopalakrishnan et al. (2013). Surface fluxes were parameterized using the exchange coefficients based on recent observational studies from field and laboratory experiments (Powell et al. 2003; Zhang et al. 2008; Haus et al. 2010; Bell et al. 2012). The Geophysical Fluid Dynamics Laboratory longwave radiation scheme following Fels and Schwarzkopf (1975) and Schwarzkopf and Fels (1991), as well as the shortwave radiation scheme of Lacis and Hansen (1974), were used. The Ferrier microphysics scheme (Ferrier et al. 2002) was also used. The simplified Arakawa–Schubert (SAS) scheme (Pan and Wu 1995; Hong and Pan 1998) was used only for the two domains at resolutions of 27 and 9 km following Gopalakrishnan et al. (2013).

The boundary layer scheme used in HWRF is the modified Medium-Range Forecast scheme (Troen and Marht 1986; Hong and Pan 1996), but it is referred to as the GFS scheme by the HWRF community (Gopalakrishnan et al. 2013; Tallapragada et al. 2014). Turbulent fluxes are parameterized through the vertical eddy diffusivity and the vertical gradient of the mean quantities. For instance, the momentum flux or wind stress τ is parameterized as

$$\tau/\rho = K_m \partial u/\partial z, \quad (1)$$

where ρ is the air density, u is the wind speed, and K_m is the vertical eddy diffusivity. The variable K_m is parameterized in the form of

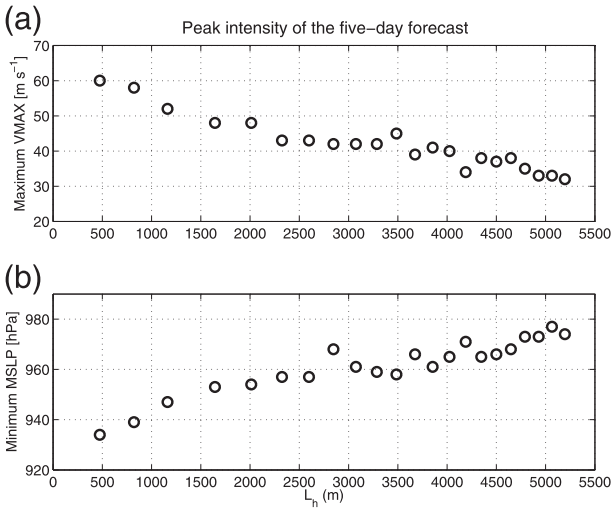

FIG. 1. Simulated maximum intensity in terms of (a) maximum wind speed and (b) minimum sea level pressure (MSLP) during each 5-day simulation as a function of L_h. VMAX is defined as the maximum 10-m wind speed at each forecast hour.

$$K_m = \kappa(u^*/F)z(1 - z/h)^2, \tag{2}$$

where $\kappa = 0.4$ is the von Kármán constant, u^* is the surface frictional velocity, F is the stability function evaluated at the top of the surface layer, z is the height above the surface, and h is the boundary height determined using the critical Richardson number (Hong and Pan 1996). During a physics upgrade (Zhang et al. 2012), a parameter α was added to Eq. (2) to control the magnitude of K_m as follows

$$K_m = k(u^*/F)z[\alpha(1 - z/h)^2]. \tag{3}$$

Note that when $\alpha = 1$, Eq. (3) is equivalent to Eq. (2). In the operational HWRF after 2012, α was set to 0.5 based on extensive tests conducted using retrospective simulations of all the storms in the 2010–11 seasons[1] (Tallapragada et al. 2014).

For horizontal diffusion, HWRF uses a first-order nonlinear Smagorinsky-type parameterization (Janjić 1990). The horizontal turbulent momentum flux F_h is typically parameterized using the eddy diffusivity K_h in the form of

$$F_h = \rho K_h S_h, \tag{4}$$

where S_h is the horizontal strain rate of the mean flow (e.g., Stevens et al. 1999) defined as

[1] As noted by Zhang et al. (2012) and Gopalakrishnan et al. (2013), $\alpha = 0.25$ matches best with observations of K_m in idealized HWRF simulations.

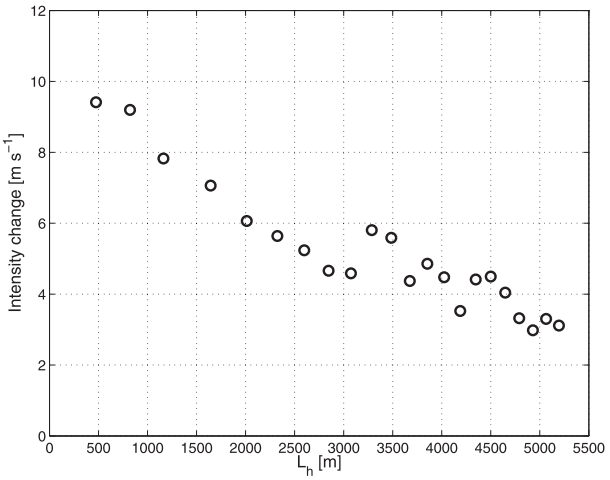

FIG. 2. Plot of the mean 24-h intensity change as a function of L_h.

$$S_h = \left(\frac{\partial v}{\partial x} + \frac{\partial u}{\partial y}\right), \tag{5}$$

where x and y are the distances in the longitudinal and latitudinal directions, respectively, and u and v are the velocity components in the longitudinal and latitudinal directions, respectively. The horizontal eddy diffusivity K_h is flow dependent and is parameterized as

$$K_h = L_h^2 D_h, \tag{6}$$

where L_h is the horizontal mixing length and D_h is the deformation defined as

$$D_h^2 = \left(\frac{\partial v}{\partial x} + \frac{\partial u}{\partial y}\right)^2 + \left(\frac{\partial u}{\partial x} - \frac{\partial v}{\partial y}\right)^2. \tag{7}$$

The first term on the right-hand side of Eq. (7) represents deformation due to shearing and is equal to the strain rate squared. The second term of Eq. (7) represents deformation due to stretching. In addition, the horizontal eddy diffusivities for heat (K_t) and moisture (K_q) are set to equal that for momentum (i.e., $K_t = K_q = K_h$) in HWRF.

In this study, to investigate the effect of horizontal diffusion on TC intensity and structure in a three-dimensional full-physics model, we conducted 23 experiments by varying L_h. Note that all the experiments were run with the same initialization and physics options, except for varying L_h.

3. Results

Figures 1a and 1b show the maximum surface wind speed and minimum sea level pressure, respectively, for each 5-day forecast of the 23 experiments as a function

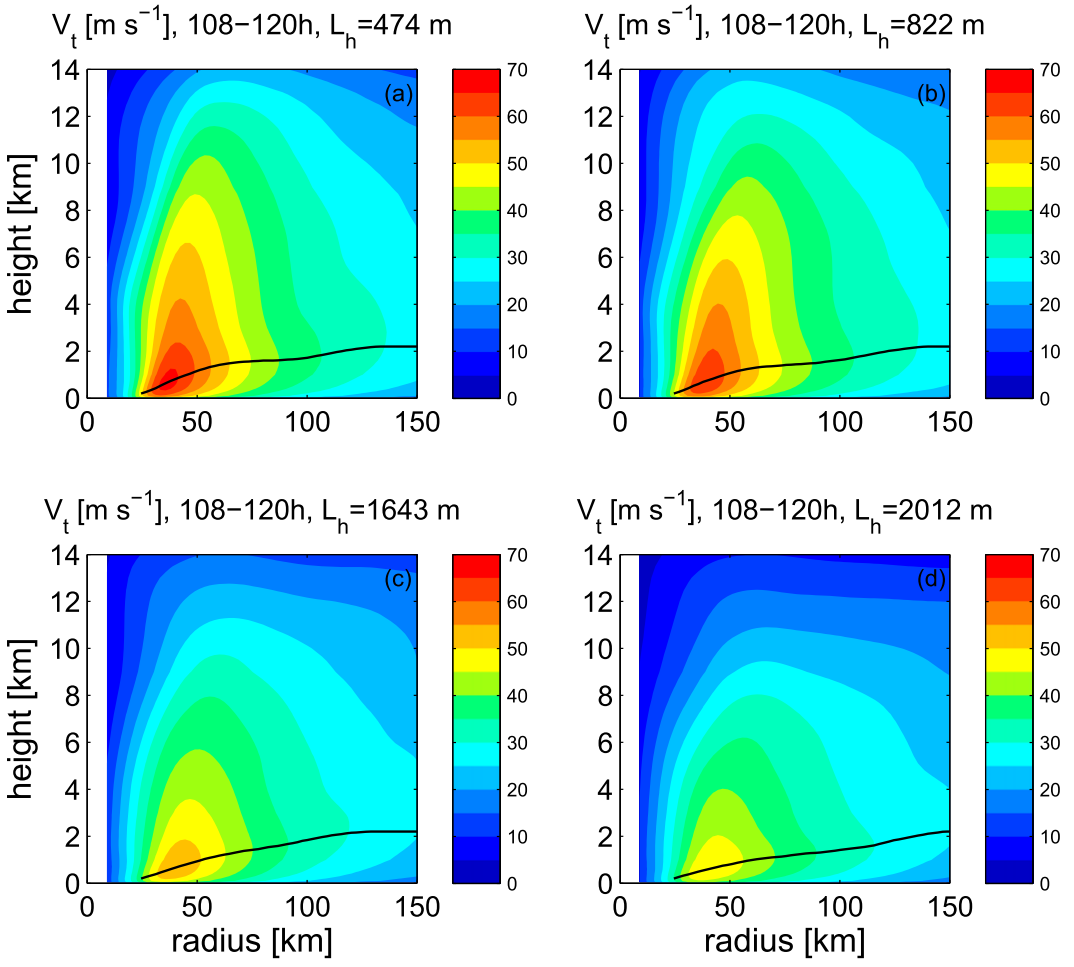

FIG. 3. Radius–height plots of the azimuthally averaged tangential velocity over the last 12 h of the 5-day simulations for L_h = (a) 474, (b) 822, (c) 1643, and (d) 2012 m. The black line represents the height of the maximum tangential velocity.

of L_h. As shown in Figs. 1a and 1b, peak intensity decreases with increasing L_h. This result is consistent with previous studies such as BR09. It also appears that peak intensity is more sensitive to smaller values of L_h. When L_h increases to the model horizontal resolution of 3 km and larger, the peak intensity becomes less sensitive to L_h. This behavior indicates that the effect of L_h on simulated peak intensity is larger when L_h is smaller than the model's horizontal resolution of the inner nest grid scales. This result is consistent with that of BR09, who showed that maximum intensity was more sensitive to smaller L_h.

In addition to peak intensity, we also investigated if intensity change is affected by horizontal mixing processes. Figure 2 shows the mean 24-h intensity change for the 5-day forecasts of all the simulations as a function of L_h. It appears that the storms with smaller L_h tend to intensify faster than those with larger L_h. We will show that the eddy transport of angular momentum plays an important role in the simulations with lower L_h. Note that rapid intensification occurred between 24 and 36 h for all the simulations before intensity leveled off at 48 h. The storms slowly reintensify after 48 h and reach a nearly steady state at the end of the 5-day simulation.

We next studied structural differences in the simulations with different L_h values when the storms reached their peak intensity during the 5-day forecasts. As an example, the radius–height representation of the azimuthally averaged tangential velocity V_t is shown in Figs. 3a–d for the simulations with L_h = 474, 822, 1643, and 2012 m, respectively. Each field is averaged between 108 and 120 h, when the simulated storm is in a nearly steady-state phase. Figure 3 shows that the V_t maximum known as the boundary layer jet is located at ~40-km radius and ~800-m altitude for all four simulations. This

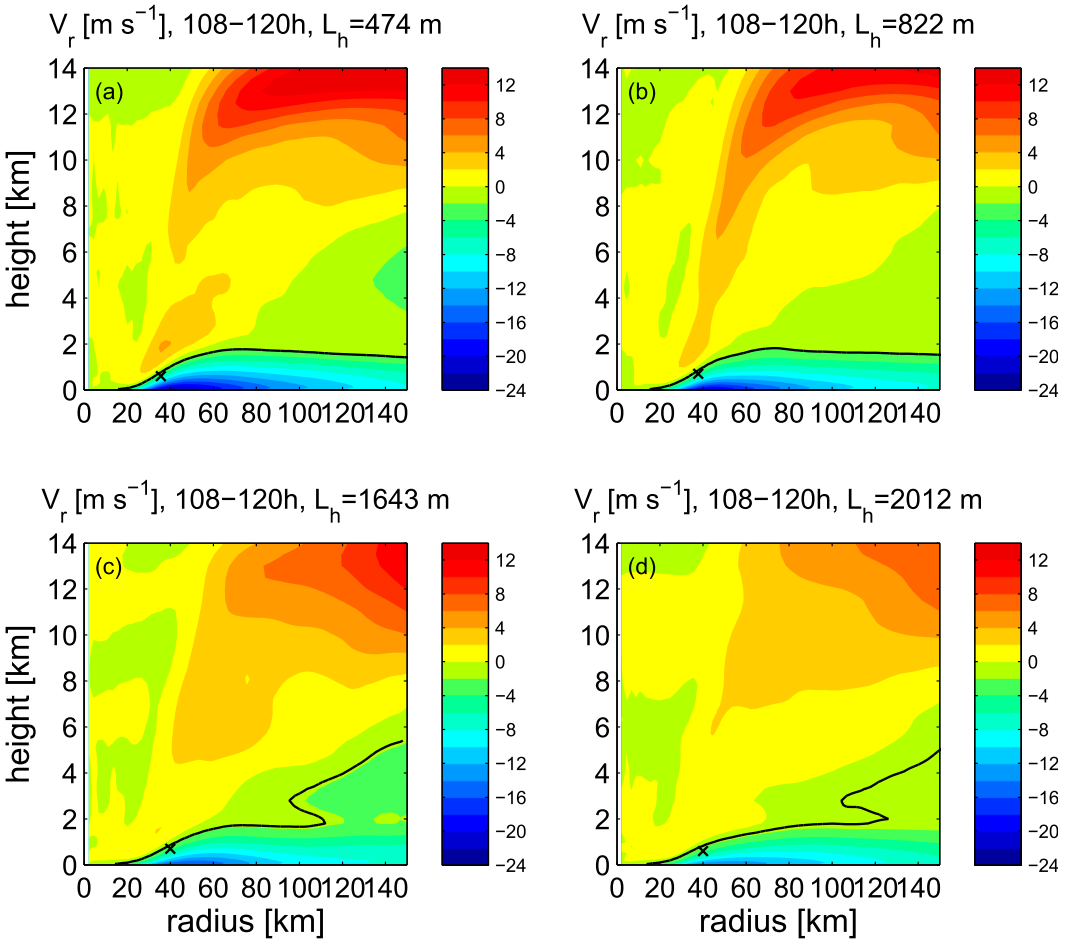

FIG. 4. As in Fig. 3, but for the radial velocity. The black line shows the inflow layer depth defined as the height of the 10% peak inflow. The black crisscross denotes the location of maximum tangential wind speed.

wind maximum or "azimuthal jet" was found in many previous observational and numerical studies in both individual and mean wind profiles (e.g., Kepert 2001; Franklin et al. 2003; Kepert 2006a, 2006b; Bell and Montgomery 2008; Nolan et al. 2009b; Zhang et al. 2011b). The TC boundary layer jet is one of the distinct features that is different from a typical boundary layer in non-TC conditions. A broad wind maximum is found at the altitude below 1 km for all the simulations, consistent with the observational composite of Zhang et al. (2011b). The peak V_t in the simulation with $L_h = 2012$ m is 45 m s^{-1}, much smaller than that (67 m s^{-1}) in the simulation with $L_h = 474$ m. It is also found that V_t outside of the radius of maximum wind speed (RMW) is broader in the simulations with larger L_h.

Figure 4 shows azimuthally averaged radial velocity V_r as a function of radius and altitude for the same four experiments in Fig. 3. The peak radial inflow is found to be located ~150 m above the sea surface. The magnitude of V_r decreases gradually with height. This structure is generally consistent with the observations of Zhang et al. (2011b). Figure 4 indicates that the peak V_r tends to decrease with increasing L_h, consistent with the decrease in intensity. The height of the inflow layer also varies from run to run. Above 1500 m near the radius of maximum wind speed, a pronounced outflow jet is evident for $L_h = 474$ m. This outflow jet is not as clear for larger L_h, indicating the outflow immediately above the inflow layer is stronger for smaller L_h.

Figs. 3 and 4 indicate that the depth of the inflow layer [defined in Zhang et al. (2011b), where V_r is equal to 10% of the peak inflow] is above the height of the maximum V_t. This behavior of the boundary layer flow is consistent with the observations of Zhang et al. (2011b), as well as with modeling studies (e.g., Kepert and Wang 2001; Nolan et al. 2009b). It is also evident that the inflow layer depth and the height of the maximum wind speed both tend to decrease with decreasing radius, especially near the core, also consistent with observations (Zhang et al. 2011b).

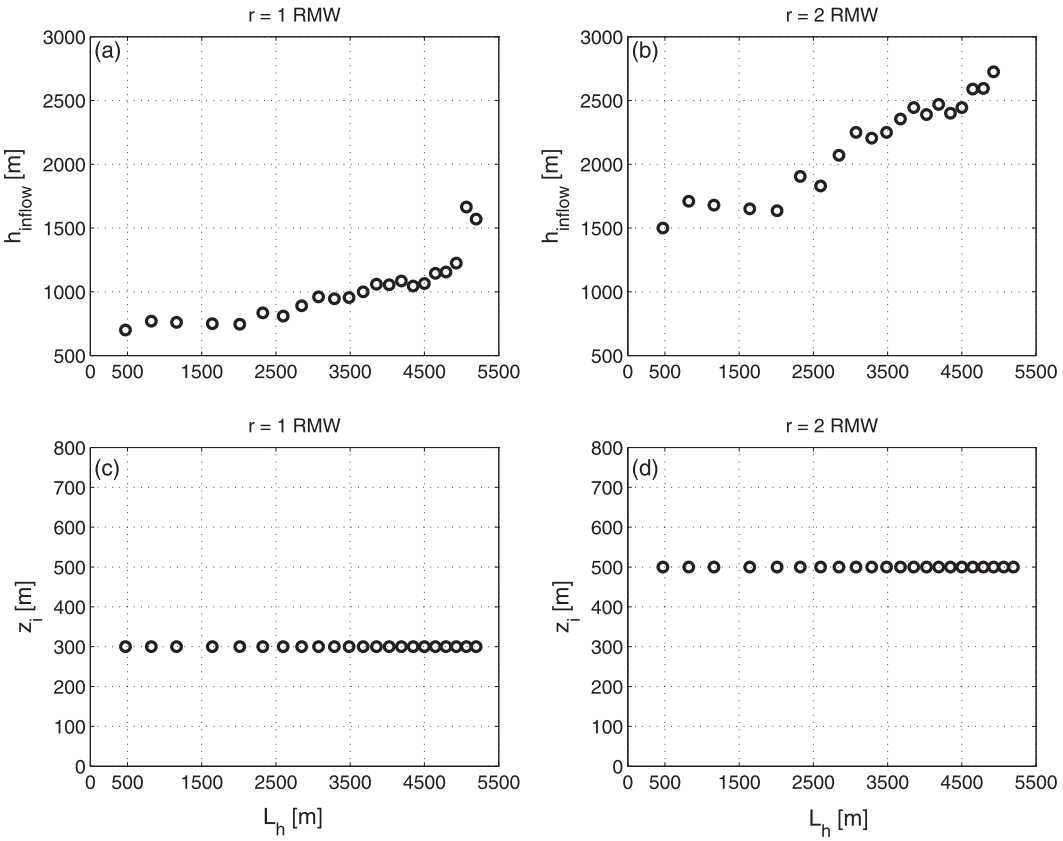

FIG. 5. Plots of (top) inflow layer depth and (bottom) mixed layer depth as a function of L_h at the location of the (a),(c) RMW and (b),(d) 2 times the RMW averaged over the last 12 h of the 5-day simulations. The inflow layer depth is defined as 10% of the peak inflow following Zhang et al. (2011b).

The inflow layer depth is found to increase with increasing L_h (Figs. 5a,b). Compared to the observations of Zhang et al. (2011b), the simulations with small L_h (<1000 m) are more consistent with observed inflow layer depths in the eyewall region than with the other simulations. Note that the horizontal mixing length estimated by ZM12 is ~750 m, which is independent of the wind speed at ~500-m altitude. It is encouraging to note that the simulation with L_h closer to that of the observed estimate produces a better structure in terms of boundary layer height than the other simulations. The thermodynamic mixed layer depth, defined as the height where virtual potential temperature changes 0.5 K from the mean of the lowest 150-m data, is also shown in Fig. 5. It is evident from Figs. 5c and 5d that the simulated mixed layer depth is not affected by the value of L_h.

The peak azimuthally averaged tangential and radial wind velocities are clearly a function of L_h. As shown in Figs. 6a and 6b, respectively, the peak V_t and V_r increase with decreasing L_h. This is expected because it was shown earlier that storm intensity is a function of L_h, and maximum V_t and V_r are typically correlated with storm intensity. Figure 6c shows the maximum vertical velocity at a 10-km altitude for each simulation as a function of L_h. The maximum vertical velocity decreases as L_h increases. This is expected since stronger storms tend to have stronger peak updrafts. It will be shown that horizontal diffusion limits the convergence of flow in the boundary layer, which is responsible for the weaker updrafts in the simulations with larger L_h. Of note, the inflow angle, defined as $\tan^{-1}(V_r/V_t)$, is not affected much by L_h (Fig. 6d), although previous work has shown that the inflow angle is affected by vertical eddy diffusivity (Zhang et al. 2012). Compared to the observed surface inflow angles given by Zhang and Uhlhorn (2012), all simulations show good agreement (i.e., within the error bar of observations).

The horizontal mixing length also tends to affect the size of the storm. Figure 7 shows the RMW at 2-km altitude as a function of L_h averaged during the last 12 h of each simulation. There is a small tendency for RMW to increase with increasing L_h, especially for $L_h > 2000$ m. Gopalakrishnan et al. (2013) found that vertical diffusion had a larger impact on the size of the storm in

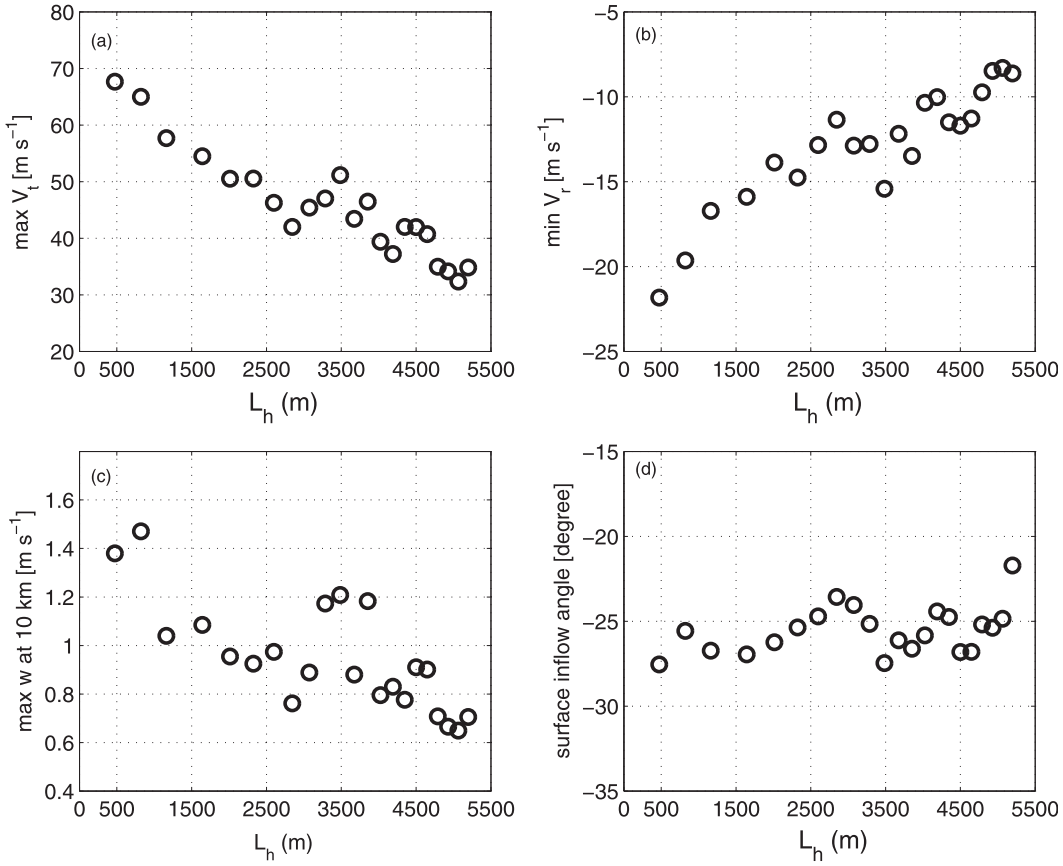

FIG. 6. Maximum azimuthally averaged (a) tangential velocity V_t, (b) radial velocity V_r, (c) vertical velocity at 10-km altitude, and (d) surface inflow angle averaged over the last 12 h of the 5-day simulations as a function L_h.

idealized HWRF simulations than the effect of the horizontal mixing lengths studied here.

Figure 8a shows the eyewall slope[2] as a function of L_h averaged for the 108–120-h simulations. There is a tendency for the eyewall slope to increase with increasing L_h, especially for larger slopes. Stern and Nolan (2009) showed that the slope of the eyewall is nearly a linear function of the size of the storm. Our results are generally consistent with the observational results of Stern and Nolan (2009) and Stern et al. (2014), who showed the eyewall slope is nearly a linear function of the RMW (Fig. 8b). The effect of L_h on the eyewall slope is thus mainly associated with changes in the size of the storm.

Budget analyses of the absolute angular momentum ($M = rV_t + 2fr^2$, where r is radial distance and f is the Coriolis frequency) are performed to elucidate the mechanisms that might contribute to intensity and structure change. The budget equation of the azimuthally averaged M tendency is given by

$$\frac{\partial\langle M\rangle}{\partial t} = -\langle V_r\rangle\frac{\partial\langle M\rangle}{\partial r} - \langle w\rangle\frac{\partial\langle M\rangle}{\partial z} - \left\langle V_r'\frac{\partial M'}{\partial r}\right\rangle - \left\langle w'\frac{\partial M'}{\partial z}\right\rangle + F_r, \quad (8)$$

where w is the vertical velocity. The brackets denote an azimuthal average at constant height, and the primes denote a departure from the azimuthal mean (or eddy). Note that all velocities in Eq. (8) are storm relative. The terms on the right-hand side of Eq. (8) are, respectively, the mean radial advection of $\langle M\rangle$, the mean vertical advection of $\langle M\rangle$, the radial advection of the resolvable eddy angular momentum, the vertical advection of the resolvable eddy angular momentum, and the combined diffusive and boundary layer tendency (F_r).[3] To investigate the role of L_h in modulating the gain/loss of $\langle M\rangle$, the total mean advection of $\langle M\rangle$ and the sum of the eddy terms were calculated and compared with the tendency of $\langle M\rangle$ and the F_r term.

[2] The eyewall slope is calculated by a linear fit of the RMW from 2 to 8 km following Stern and Nolan (2009).

[3] The F_r term is the combination of the vertical and horizontal diffusion caused by subgrid processes.

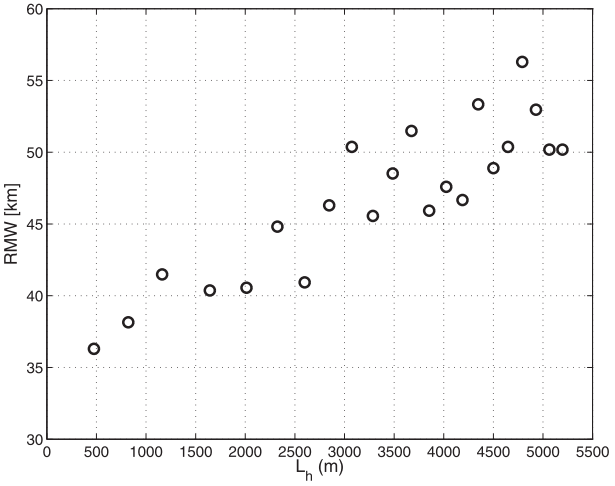

FIG. 7. Radius of maximum azimuthally averaged tangential wind speed (RMW) at 2-km altitude as a function of L_h. Each data point represents RMW averaged over the last 12 h of the 5-day simulations.

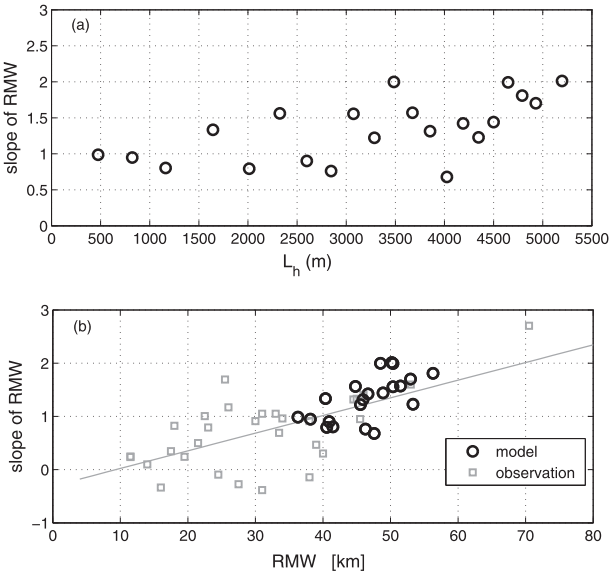

FIG. 8. (a) Eyewall slope averaged over the last 12 h of the 5-day simulations as a function of L_h; (b) eyewall slope as a function of RMW for different values of L_h. The observational data in (b) are from Stern et al. (2014).

Figure 9 shows time averages of the terms in the azimuthally averaged angular momentum of Eq. (8) during the period of rapid intensification (between 24 and 36 h) for simulations with $L_h = 474$ and 2596 m. We note that the results from these two simulations are shown as an example of the generalized findings from all simulations. The $\langle M \rangle$ tendency is found to be larger for smaller L_h in the eyewall region (Figs. 9a,b), which is consistent with the trend of intensity change as a function of L_h (Fig. 2).

In all simulations, the total mean advection of $\langle M \rangle$ and the F_r term are the main contributors to the gain and loss of $\langle M \rangle$, respectively, especially in the boundary layer (Figs. 9c,d and Figs. 9g,h). These two variables are similar in structure but of largely opposite sign so that the total $\langle M \rangle$ tendency is small (Figs. 9a,b). As expected, the larger the L_h, the larger the magnitude of the negative F_r term. The spinup of the vortex in the boundary layer is mainly due to the positive mean advection of $\langle M \rangle$ that is mainly from the horizontal mean advection component or the convergence of $\langle M \rangle$. The convergence of $\langle M \rangle$ exceeds the boundary layer friction and diffusion caused by subgrid processes, which is consistent with the spinup theory of Smith et al. (2009) that emphasized the importance of the boundary layer spinup mechanism.

In the simulation with larger L_h, the total mean advection of $\langle M \rangle$ contributes much more to the total tendency than the resolvable eddy transport (Figs. 9c,d) and opposes the larger F_r or subgrid tendencies. On the other hand, the resolved eddy contribution to the total $\langle M \rangle$ tendency becomes much more important in the simulation with smaller L_h. The magnitude of the resolved eddy contribution can be as large as that of the total mean advection or the F_r term when L_h is small (Fig. 9e). The role of the resolved eddies is to sharpen the radial gradient of M near the eyewall region because the sign of the total mean eddy term is opposite on each side of the RMW. The positive eddy transport of $\langle M \rangle$ inward from the RMW at low levels is responsible for the spinup of the vortex when L_h is small. This large positive eddy transport of $\langle M \rangle$ also cancels the negative mean advection of $\langle M \rangle$ right above the boundary layer where the outflow jet takes place in the simulation with small L_h. Of note, the unresolved eddies, although relatively small, also positively contribute to the total tendency of $\langle M \rangle$ above the boundary layer when L_h is small (Fig. 9g). This result indicates the important role of L_h in regulating the relative contributions to the total tendency of $\langle M \rangle$ from the resolved and unresolved eddies.

To illustrate the features of the resolved eddies, Fig. 10 shows the horizontal view of the vertical velocity and relative vorticity fields at 1-km altitude at 24 h for the same two simulations shown in Fig. 9. The vertical velocity and relative vorticity fields are much smoother in the simulation with larger L_h. The downward motion with larger magnitude covers a larger fraction of the whole domain in the simulation with larger L_h, especially between the eyewall and the outer rainbands (Figs. 10a,b). For all simulations, large values of cyclonic vorticity are mainly concentrated near the center of the storm with curved band features tied to the edge of the maximum (Figs. 10c,d). In the simulation with smaller L_h, there are more features with weak cyclonic/anticyclonic vorticity (Fig. 10c). These eddies are believed to be

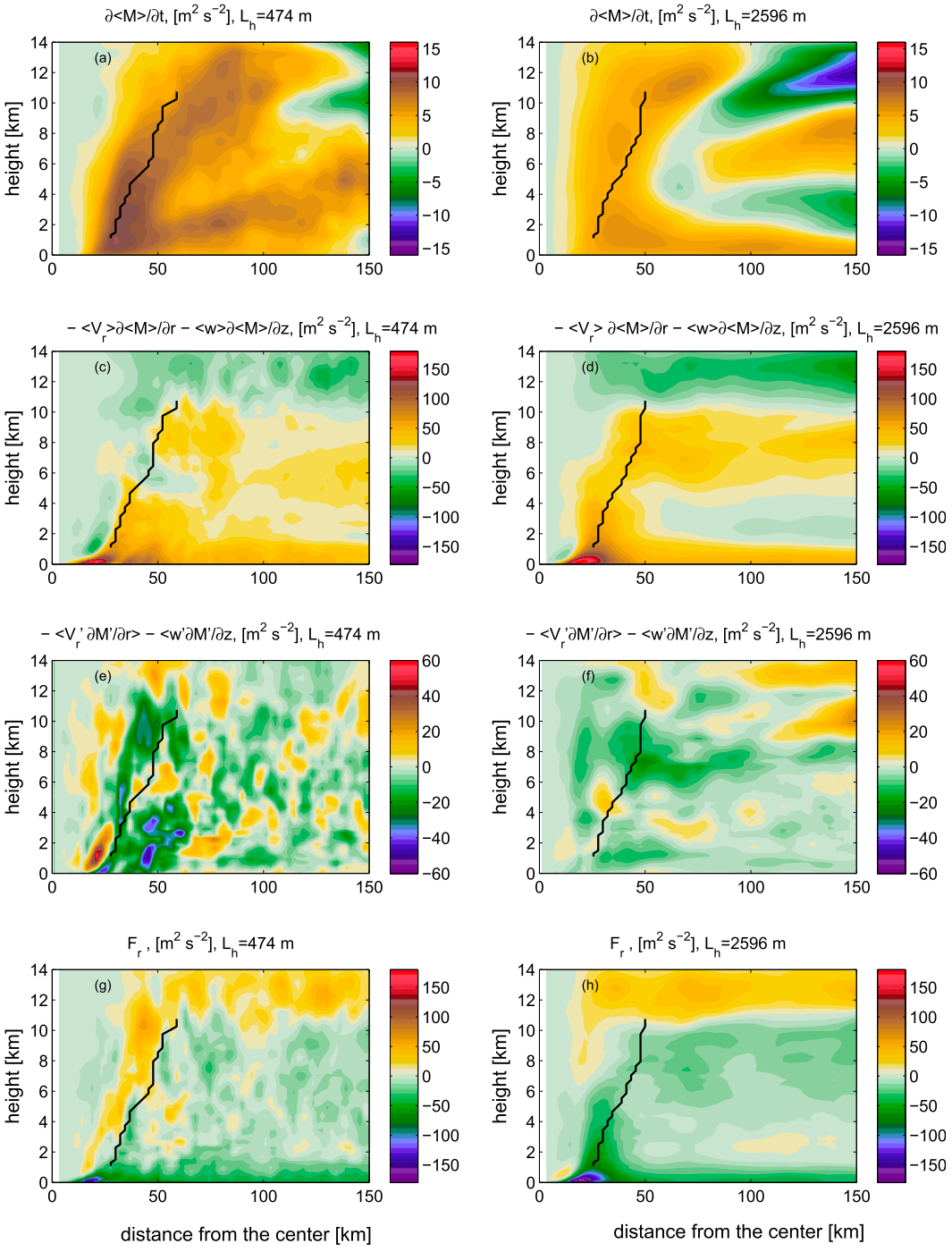

FIG. 9. Radius–height plots of the terms in the azimuthally averaged absolute angular momentum ($\langle M \rangle$) budget for simulations with L_h = (left) 474 and (right) 2596 m during a period of rapid intensification (between 24 and 36 h). These budget terms include (a),(b) the local rate of change of ($\langle M \rangle$); (c),(d) the total mean advection; (e),(f) the sum of the eddy transport of ($\langle M \rangle$); and (g),(h) the friction term F_r. The black line represents the radius of maximum azimuthally averaged tangential wind speed.

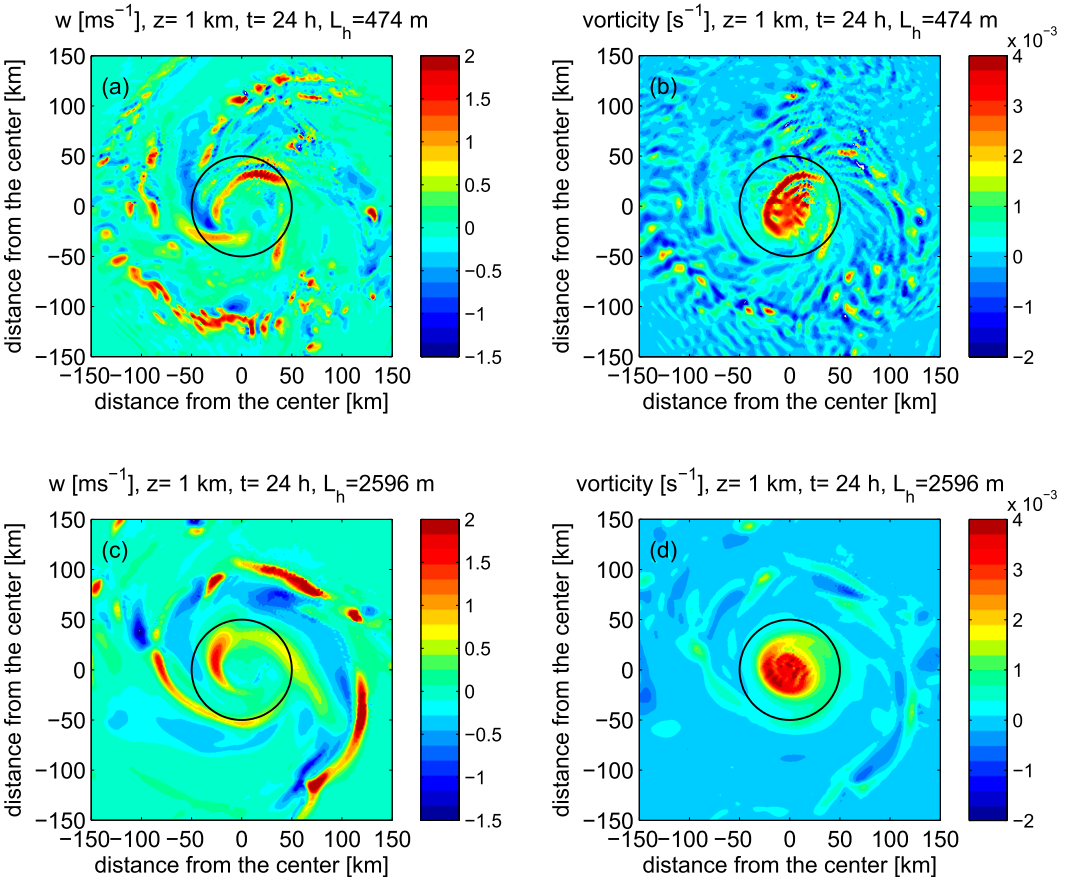

FIG. 10. Horizontal view of the (left) vertical velocity and (right) relative vorticity at the height of 1 km at 24 h from the initial time for simulations with L_h = (a),(b) 474 and (c),(d) 2596 m. The black line represents a radius of 50 km.

responsible for the large eddy transport of angular momentum in the angular momentum budget observed in Fig. 9.

Figure 11 shows the horizontal map of equivalent potential temperature θ_e at the altitude of 1 km and 100 m at 24 h from the initial time from the same simulations shown in Fig. 9. It is evident from Fig. 11 that the boundary layer θ_e is much lower in the outer-core region in the simulation with larger L_h. This low-θ_e air in the boundary layer is collocated with the strong downward motion seen in Fig. 10b, suggesting convective and mesoscale downdrafts bring down low-θ_e air into the boundary layer from the upper levels. This result indicates that L_h also affects thermodynamic structure through the coupling between the boundary layer processes and convection.

4. Discussion and conclusions

In this study, we examined the effects of horizontal diffusion on TC intensity and structure in idealized numerical simulations using the HWRF. Horizontal mixing lengths (L_h) ranging from 0 to ~5 km were varied in sensitivity experiments, while keeping the vertical diffusion coefficient, sea surface temperature, and other physical parameterizations the same. Our results show that simulated maximum intensity and intensity change are more sensitive to smaller L_h, consistent with the results of BR09. The simulated mean rate of the change of intensity and maximum 5-day forecasted intensity are larger for simulations with smaller L_h.

The sensitivity experiments demonstrated that L_h is strongly related to the dynamic, but not the thermodynamic, boundary layer height. Zhang et al. (2012) and Gopalakrishnan et al. (2013) found that vertical diffusion had a large impact on simulations of the dynamical boundary layer height. It is interesting to note that horizontal diffusion is also linked to the dynamical boundary layer height. The reason for the increase in kinematic boundary layer height is related to the modification of horizontal mixing and, subsequently, the inertial stability. As found by Kepert (2001), the dynamical boundary layer height h, or the height of boundary layer jet, is a function of inertial stability I and vertical diffusion coefficient K_m in the form of

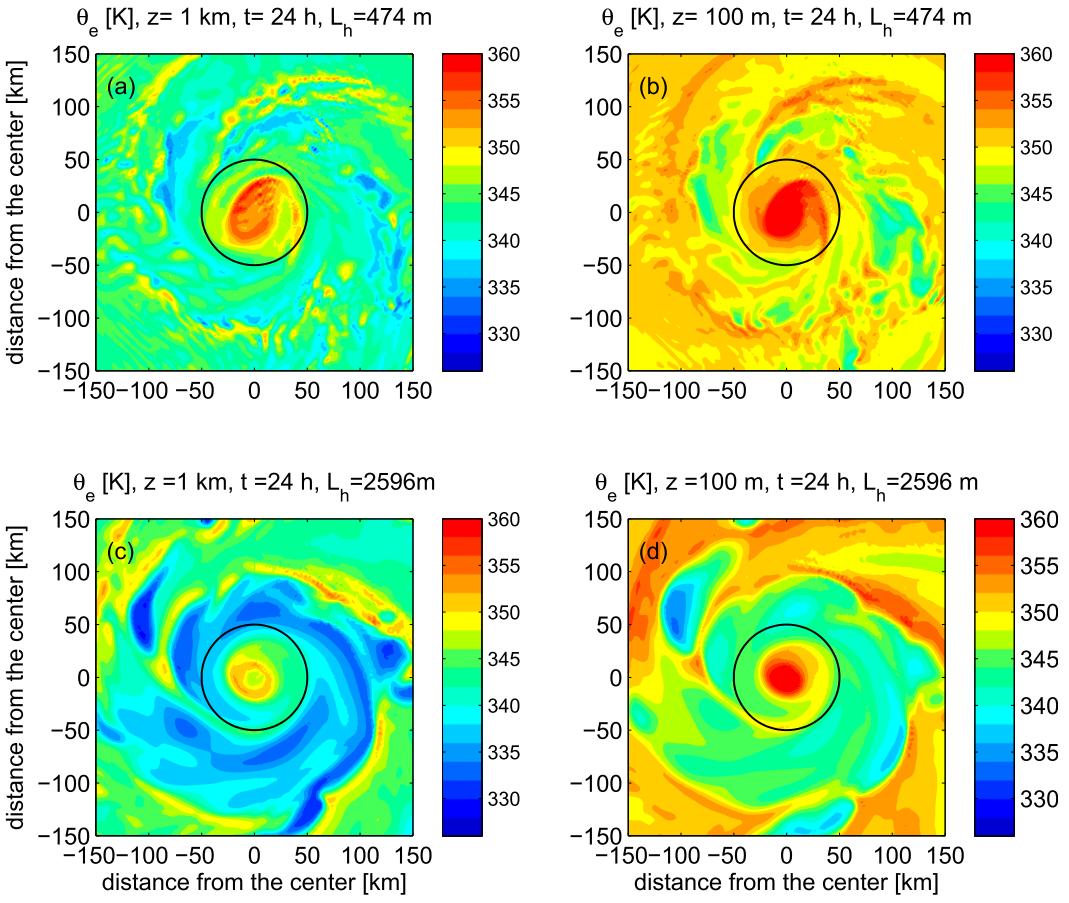

FIG. 11. Horizontal view of the equivalent potential temperature at the heights of (left) 1 km and (right) 100 m at 24 h from the initial time for simulations with L_h = (a),(b) 474 and (c),(d) 2596 m. The black line represents a radius of 50 km.

$$h = (2K_m/I)^{1/2}. \tag{9}$$

Note that the inertial stability is defined as

$$I^2 = (f + V_t/r + \partial V_t/\partial r)(f + 2V_t/r). \tag{10}$$

When the vertical diffusion is constant, the main influence on the boundary layer height is from inertial stability. Figure 12 shows radius–height plots of the inertial stability for different L_h, indicating that the inertial stability actually decreases with increasing L_h. Equation (9) indicates that when the inertial stability increases, the boundary layer height becomes smaller, consistent with our findings.

Our results indicate that eyewall slope increases with the horizontal mixing length. However, this increase is mainly due to the increase in the size of the storm when L_h increases. As found by Stern and Nolan (2009), eyewall slope is nearly a linear function of storm size; our results are consistent with this observation. It is also interesting to note that the near-surface inflow angle has little dependence on the horizontal mixing length, although both the peak radial and tangential wind velocities vary with L_h. Because the inflow angle represents the relative strength between the radial and tangential velocities, this result indicates that the radial and tangential components must respond to horizontal mixing in a similar manner. While the tangential velocity decreases with increasing mixing length, the magnitude of radial velocity also decreases so that the inflow angle does not change much.

The focus of this paper is on 5-day simulations of TC structure, as well as intensity change, in the framework of forecasts using an idealized version of the operational HWRF, which is somewhat different than that of BR09 and RB12. Nevertheless, our results support those of BR09 and RB12 in that the effect of horizontal mixing in three-dimensional simulations is to smooth the radial gradient of angular momentum and thermal parameters. With smaller horizontal mixing lengths, the radial wind

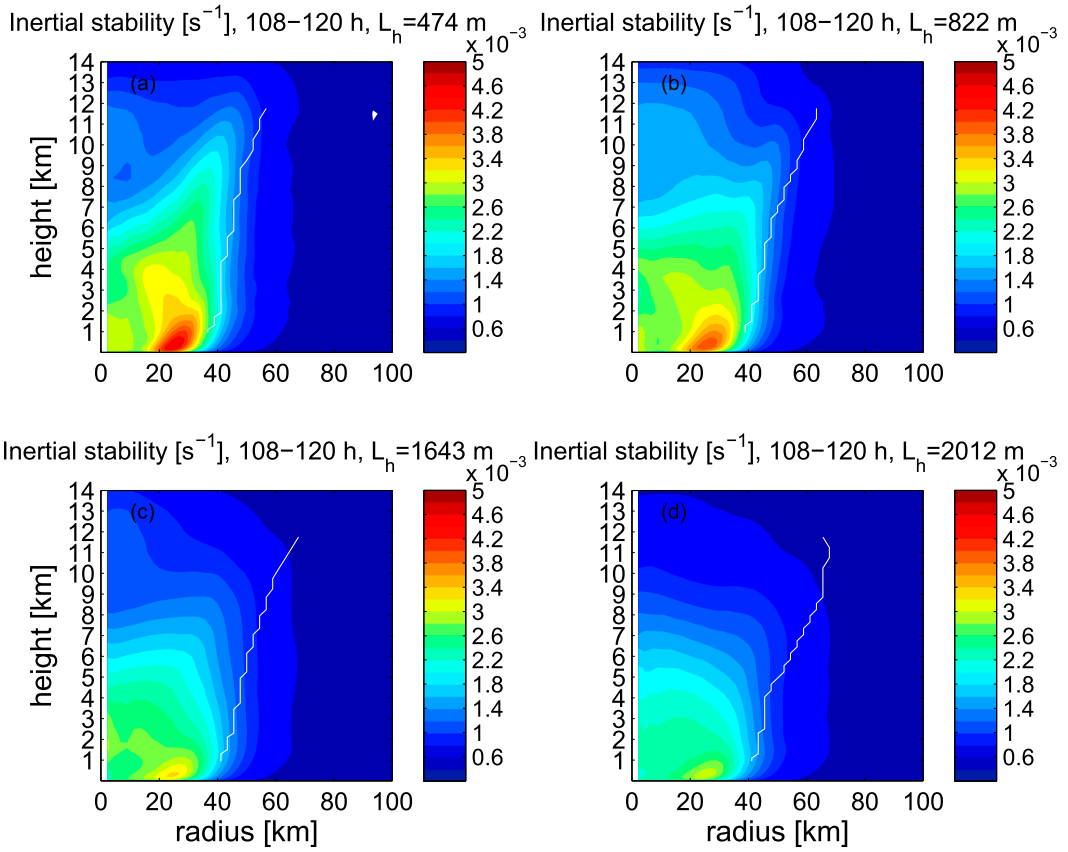

FIG. 12. Radius–height plots of the azimuthally averaged inertial stability over the last 12 h of the 5-day simulations for L_h = (a) 474, (b) 822, (c) 1643, and (d) 2012 m. The white line represents the radius of maximum azimuthally averaged tangential wind speed.

speed is much stronger in the boundary layer. The stronger radial inflow, plus the larger radial gradient of angular momentum, made the convergence of the angular momentum larger for smaller horizontal mixing lengths.

Angular momentum budget analyses during the intensification phase suggest that the eddy transport of angular momentum contributes substantially to the total tendency of angular momentum, especially at low levels (<4 km) inside the radius of the maximum tangential wind speed when L_h is small (<1000 m). Our results are in agreement with those of Persing et al. (2013), who pointed out that under certain conditions the eddy momentum flux could be important for the spinup of the tangential wind velocity in three-dimensional numerical simulations compared to axisymmetric model simulations. Previous studies of three-dimensional numerical simulations of tropical cyclones also found that resolved eddies tended to spin down the tangential wind speed in the boundary layer of the eyewall region, while spinning up the tangential wind speed inside the RMW (Wang 2002; Wu and Braun 2004; Yang et al. 2007). Based on our results, these studies likely used small horizontal mixing lengths (<1000 m).

The thermodynamic structure in the boundary layer is also found to be different between the simulations with different values of L_h. In the simulation with larger L_h, relatively low-θ_e air is found in the boundary layer of the outer-core region, an area associated with more organized and stronger downdrafts. As noted by Powell (1990) and Riemer et al. (2010), low-θ_e air in the boundary layer close to the rainbands or eyewall region acts to retard storm intensification.

We note that the simulated maximum intensity in our simulations is smaller than that in the axisymmetric simulations of BR09 and Bryan (2012). Previous studies (Yang et al. 2007; Bryan et al. 2010; Persing et al. 2013) also found that three-dimensional model simulations tended to have a lower maximum intensity than that in axisymmetric simulations. Note that the storm size (i.e., RMW) simulated in our simulations is ~40 km, while the storm size in Bryan's simulations is ~20 km. This result indicates that the effect of L_h on maximum intensity may be dependent on storm size. Hakim (2011) showed that the effect of horizontal mixing on MPI was small when the storm size was ~80 km, supporting the above hypothesis.

Note also that both Bryan's and Hakim's simulations lasted for more than 12 days and nearly reached equilibrium, while our simulations only lasted 5 days with a tendency for the storms to slowly intensify at the end of each 5-day forecast. This may be an additional reason for the smaller maximum intensity observed in our simulations when compared to other studies.

Our results provide the first attempt to study the impact of horizontal mixing on TC intensity and structure forecasts in an operational TC model. We hope our results will provide guidance for improving the next generation of high-resolution operational TC models. Note that the current version of the HWRF uses $L_h > 2000$ m. Our results imply that a smaller L_h (<1000 m) should be used in HWRF to simulate more realistic TC structure. Real-case simulations will be run in the future to confirm the findings from this study and to determine the optimal L_h to be used in the operational HWRF following the model development framework given by Zhang et al. (2012, 2015). We also note that observational estimates of horizontal mixing are very limited at the current stage; collecting high-resolution observational data in the TC eyewall and boundary layer are critical for the modeling community to further improve the physics of operational TC models.

Acknowledgments. This work was mainly supported through the NOAA Hurricane Forecast Improvement Program (HFIP). Jun Zhang was partially supported by NOAA Grant NA14NWS4680028 and NASA Grant NNX14AM69G. We thank Sim Aberson, Eric Uhlhorn, and David Nolan for providing valuable comments and suggestions on an early version of the paper. We thank Ms. Gail Derr for offering editorial support. We also thank HWRF developers from EMC, HRD, and ESRL, especially Sundararaman Gopalakrishnan and Jian-Wen Bao, for developing the idealized system of HWRF. We are very grateful to our editor, George Bryan, and to three reviewers for their comments and suggestions that substantially improved our paper. Jun Zhang is also grateful to Paul Reasor for helpful discussions on the angular momentum budget analysis.

REFERENCES

Bao, J.-W., S. G. Gopalakrishnan, S. A. Michelson, F. D. Marks Jr., and M. T. Montgomery, 2012: Impact of physics representations in the HWRFX on simulated hurricane structure and pressure–wind relationships. *Mon. Wea. Rev.*, **140**, 3278–3299, doi:10.1175/MWR-D-11-00332.1.

Bell, M. M., and M. T. Montgomery, 2008: Observed structure, evolution, and intensity of category five Hurricane Isabel (2003) from 12 to 14 September. *Mon. Wea. Rev.*, **136**, 2023–2036, doi:10.1175/2007MWR1858.1.

——, ——, and K. A. Emanuel, 2012: Air–sea enthalpy and momentum exchange at major hurricane wind speeds observed during CBLAST. *J. Atmos. Sci.*, **69**, 3197–3222, doi:10.1175/JAS-D-11-0276.1.

Braun, S. A., and W.-K. Tao, 2000: Sensitivity of high-resolution simulations of Hurricane Bob (1991) to planetary boundary layer parameterizations. *Mon. Wea. Rev.*, **128**, 3941–3961, doi:10.1175/1520-0493(2000)129<3941:SOHRSO>2.0.CO;2.

Bryan, G. H., 2012: Effects of surface exchange coefficients and turbulence length scales on the intensity and structure of numerically simulated hurricanes. *Mon. Wea. Rev.*, **140**, 1125–1143, doi:10.1175/MWR-D-11-00231.1.

——, and R. Rotunno, 2009: The maximum intensity of tropical cyclones in axisymmetric numerical model simulations. *Mon. Wea. Rev.*, **137**, 1770–1789, doi:10.1175/2008MWR2709.1.

——, ——, and Y. Chen, 2010: The effects of turbulence on hurricane intensity. *29th Conf. on Hurricanes and Tropical Meteorology*, Tucson, AZ, Amer. Meteor. Soc., 8C.7. [Available online at https://ams.confex.com/ams/29Hurricanes/webprogram/Paper167282.html.]

Emanuel, K. A., 1995: Sensitivity of tropical cyclones to surface exchange coefficients and a revised steady-state model incorporating eye dynamics. *J. Atmos. Sci.*, **52**, 3969–3976, doi:10.1175/1520-0469(1995)052<3969:SOTCTS>2.0.CO;2.

——, 1997: Some aspects of hurricane inner-core dynamics and energetics. *J. Atmos. Sci.*, **54**, 1014–1026, doi:10.1175/1520-0469(1997)054<1014:SAOHIC>2.0.CO;2.

Fels, S. B., and M. D. Schwarzkopf, 1975: The simplified exchange approximation: A new method for radiative transfer calculations. *J. Atmos. Sci.*, **32**, 1475–1488, doi:10.1175/1520-0469(1975)032<1475:TSEAAN>2.0.CO;2.

Ferrier, B. S., Y. Lin, T. Black, E. Rogers, and G. DiMego, 2002: Implementation of a new grid-scale cloud and precipitation scheme in the NCEP Eta model. *19th Conf. on Weather Analysis and Forecasting/15th Conf. on Numerical Weather Prediction*, San Antonio, TX, Amer. Meteor. Soc., 10.1. [Available online at https://ams.confex.com/ams/SLS_WAF_NWP/techprogram/paper_47241.htm.]

Foster, R. C., 2009: Boundary-layer similarity under an axisymmetric, gradient wind vortex. *Bound.-Layer Meteor.*, **131**, 321–344, doi:10.1007/s10546-009-9379-1.

Franklin, J. L., M. L. Black, and K. Valde, 2003: GPS dropwindsonde wind profiles in hurricanes and their operational implications. *Wea. Forecasting*, **18**, 32–44, doi:10.1175/1520-0434(2003)018<0032:GDWPIH>2.0.CO;2.

Gall, R., J. Franklin, F. Marks, E. N. Rappaport, and F. Toepfer, 2013: The Hurricane Forecast Improvement Project. *Bull. Amer. Meteor. Soc.*, **94**, 329–343, doi:10.1175/BAMS-D-12-00071.1.

Gopalakrishnan, S. G., F. D. Marks, X. Zhang, J.-W. Bao, K.-S. Yeh, and R. Atlas, 2011: The experimental HWRF system: A study on the influence of horizontal resolution on the structure and intensity changes in tropical cyclones using an idealized framework. *Mon. Wea. Rev.*, **139**, 1762–1784, doi:10.1175/2010MWR3535.1.

——, S. Goldenberg, T. Quirino, F. D. Marks Jr., X. Zhang, K.-S. Yeh, R. Atlas, and V. Tallapragada, 2012: Toward improving high-resolution numerical hurricane forecasting: Influence of model horizontal grid resolution, initialization, and physics. *Wea. Forecasting*, **27**, 647–666, doi:10.1175/WAF-D-11-00055.1.

——, F. D. Marks, Jr., J. A. Zhang, X. Zhang, J.-W. Bao, and V. Tallapragada, 2013: A study of the impacts of vertical diffusion on the structure and intensity of the tropical cyclones using the high resolution HWRF system. *J. Atmos. Sci.*, **70**, 524–541, doi:10.1175/JAS-D-11-0340.1.

Gray, W. M., E. Ruprecht, and R. Phelps, 1975: Relative humidity in tropical weather systems. *Mon. Wea. Rev.*, **103**, 685–690, doi:10.1175/1520-0493(1975)103<0685:RHITWS>2.0.CO;2.

Hakim, G. J., 2011: The mean state of axisymmetric hurricanes in statistical equilibrium. *J. Atmos. Sci.*, **68**, 1364–1376, doi:10.1175/2010JAS3644.1.

Haus, B. K., D. Jeong, M. A. Donelan, J. A. Zhang, and I. Savelyev, 2010: Relative rates of sea-air heat transfer and frictional drag in very high winds. *Geophys. Res. Lett.*, **37**, L07802, doi:10.1029/2009GL042206.

Hong, S.-Y., and H.-L. Pan, 1996: Nonlocal boundary layer vertical diffusion in a Medium-Range Forecast Model. *Mon. Wea. Rev.*, **124**, 2322–2339, doi:10.1175/1520-0493(1996)124<2322:NBLVDI>2.0.CO;2.

——, and ——, 1998: Convective trigger function for a mass-flux cumulus parameterization scheme. *Mon. Wea. Rev.*, **126**, 2599–2620, doi:10.1175/1520-0493(1998)126<2599:CTFFAM>2.0.CO;2.

Janjić, Z. I., 1990: The step-mountain coordinate: Physical package. *Mon. Wea. Rev.*, **118**, 1429–1443, doi:10.1175/1520-0493(1990)118<1429:TSMCPP>2.0.CO;2.

Kepert, J. D., 2001: The dynamics of boundary layer jets within the tropical cyclone core. Part I: Linear theory. *J. Atmos. Sci.*, **58**, 2469–2484, doi:10.1175/1520-0469(2001)058<2469:TDOBLJ>2.0.CO;2.

——, 2006a: Observed boundary layer wind structure and balance in the hurricane core. Part I: Hurricane Georges. *J. Atmos. Sci.*, **63**, 2169–2193, doi:10.1175/JAS3745.1.

——, 2006b: Observed boundary layer wind structure and balance in the Hurricane core. Part II: Hurricane Mitch. *J. Atmos. Sci.*, **63**, 2194–2211, doi:10.1175/JAS3746.1.

——, 2010: Slab- and height-resolving models of the tropical cyclone boundary layer. Part I: Comparing the simulations. *Quart. J. Roy. Meteor. Soc.*, **136**, 1686–1699, doi:10.1002/qj.667.

——, 2012: Choosing a boundary layer parameterization for tropical cyclone modeling. *Mon. Wea. Rev.*, **140**, 1427–1445, doi:10.1175/MWR-D-11-00217.1.

——, and Y. Wang, 2001: The dynamics of boundary layer jets within the tropical cyclone core. Part II: Nonlinear enhancement. *J. Atmos. Sci.*, **58**, 2485–2501, doi:10.1175/1520-0469(2001)058<2485:TDOBLJ>2.0.CO;2.

Lacis, A. A., and J. E. Hansen, 1974: A parameterization for the absorption of solar radiation in the Earth's atmosphere. *J. Atmos. Sci.*, **31**, 118–133, doi:10.1175/1520-0469(1974)031<0118:APFTAO>2.0.CO;2.

Nolan, D. S., J. A. Zhang, and D. P. Stern, 2009a: Evaluation of planetary boundary layer parameterizations in tropical cyclones by comparison of in-situ data and high-resolution simulations of Hurricane Isabel (2003). Part I: Initialization, maximum winds, and outer core boundary layer structure. *Mon. Wea. Rev.*, **137**, 3651–3674, doi:10.1175/2009MWR2785.1.

——, ——, and ——, 2009b: Evaluation of planetary boundary layer parameterizations in tropical cyclones by comparison of in-situ data and high-resolution simulations of Hurricane Isabel (2003). Part II: Inner core boundary layer and eyewall structure. *Mon. Wea. Rev.*, **137**, 3675–3698, doi:10.1175/2009MWR2786.1.

Pan, H.-L., and W.-S. Wu, 1995: Implementing a mass flux convection parameterization package for the NMC Medium-Range Forecast model. NMC Office Note 409, 40 pp. [Available online at http://www.lib.ncep.noaa.gov/ncepofficenotes/files/01408A42.pdf.]

Persing, J., and M. T. Montgomery, 2003: Hurricane superintensity. *J. Atmos. Sci.*, **60**, 2349–2371, doi:10.1175/1520-0469(2003)060<2349:HS>2.0.CO;2.

——, ——, J. C. McWilliams, and R. K. Smith, 2013: Asymmetric and axisymmetric dynamics of tropical cyclones. *Atmos. Chem. Phys.*, **13**, 12 299–12 341, doi:10.5194/acp-13-12299-2013.

Powell, M. D., 1990: Boundary layer structure and dynamics in outer hurricane rainbands. Part II: Downdraft modification and mixed layer recovery. *Mon. Wea. Rev.*, **118**, 918–938, doi:10.1175/1520-0493(1990)118<0918:BLSADI>2.0.CO;2.

——, P. J. Vickery, and T. A. Reinhold, 2003: Reduced drag coefficient for high wind speeds in tropical cyclones. *Nature*, **422**, 279–283, doi:10.1038/nature01481.

Riemer, M., M. T. Montgomery, and M. E. Nicholls, 2010: A new paradigm for intensity modification of tropical cyclones: Thermodynamic impact of vertical wind shear on the inflow layer. *Atmos. Chem. Phys.*, **10**, 3163–3188, doi:10.5194/acp-10-3163-2010.

Rotunno, R., and G. H. Bryan, 2012: Effects of parameterized diffusion on simulated hurricanes. *J. Atmos. Sci.*, **69**, 2284–2299, doi:10.1175/JAS-D-11-0204.1.

——, Y. Chen, W. Wang, C. Davis, J. Dudhia, and G. J. Holland, 2009: Large-eddy simulation of an idealized tropical cyclone. *Bull. Amer. Meteor. Soc.*, **90**, 1783–1788, doi:10.1175/2009BAMS2884.1.

Schwarzkopf, M. D., and S. B. Fels, 1991: The simplified exchange method revisited: An accurate, rapid method for computation of infrared cooling rates and fluxes. *J. Geophys. Res.*, **96**, 9075–9096, doi:10.1029/89JD01598.

Smith, R. K., M. T. Montgomery, and S. V. Nguyen, 2009: Tropical cyclone spin-up revisited. *Quart. J. Roy. Meteor. Soc.*, **135**, 1321–1335, doi:10.1002/qj.428.

Stern, D. P., and D. S. Nolan, 2009: Reexamining the vertical structure of tangential winds in tropical cyclones: Observations and theory. *J. Atmos. Sci.*, **66**, 3579–3600, doi:10.1175/2009JAS2916.1.

——, J. R. Brisbois, and D. S. Nolan, 2014: An expanded dataset of hurricane eyewall sizes and slopes. *J. Atmos. Sci.*, **71**, 2747–2762, doi:10.1175/JAS-D-13-0302.1.

Stevens, B., C. Moeng, and P. P. Sullivan, 1999: Large-eddy simulations of radiatively driven convection: Sensitivities to the representation of small scales. *J. Atmos. Sci.*, **56**, 3963–3984, doi:10.1175/1520-0469(1999)056<3963:LESORD>2.0.CO;2.

Tallapragada, V., C. Kieu, Y. Kwon, S. Trahan, Q. Liu, Z. Zhang, and I. Kwon, 2014: Evaluation of storm structure from the operational HWRF model during 2012 implementation. *Mon. Wea. Rev.*, **142**, 4308–4325, doi:10.1175/MWR-D-13-00010.1.

Troen, I., and L. Mahrt, 1986: A simple model of the atmospheric boundary layer; sensitivity to surface evaporation. *Bound.-Layer Meteor.*, **37**, 129–148, doi:10.1007/BF00122760.

Wang, Y., 1995: An inverse balance equation in sigma coordinates for model initialization. *Mon. Wea. Rev.*, **123**, 482–488, doi:10.1175/1520-0493(1995)123<0482:AIBEIS>2.0.CO;2.

——, 2002: Vortex Rossby waves in a numerically simulated tropical cyclone. Part II: The role in tropical cyclone structure and intensity changes. *J. Atmos. Sci.*, **59**, 1239–1262, doi:10.1175/1520-0469(2002)059<1239:VRWIAN>2.0.CO;2.

Wu, L., and S. A. Braun, 2004: Effect of convective asymmetries on hurricane intensity: A numerical study. *J. Atmos. Sci.*, **61**, 3065–3081, doi:10.1175/JAS-3343.1.

Yang, B., Y. Wang, and B. Wang, 2007: The effect of internally generated inner-core asymmetrics on tropical cyclone potential intensity. *J. Atmos. Sci.*, **64**, 1165–1188, doi:10.1175/JAS3971.1.

Zhang, J. A., and M. T. Montgomery, 2012: Observational estimates of the horizontal eddy diffusivity and mixing length in the low-level region of intense hurricanes. *J. Atmos. Sci.*, **69**, 1306–1316, doi:10.1175/JAS-D-11-0180.1.

——, and E. W. Uhlhorn, 2012: Hurricane sea surface inflow angle and an observation-based parametric model. *Mon. Wea. Rev.*, **140**, 3587–3605, doi:10.1175/MWR-D-11-00339.1.

——, P. G. Black, J. R. French, and W. M. Drennan, 2008: First direct measurements of enthalpy flux in the hurricane boundary layer: The CBLAST results. *Geophys. Res. Lett.*, **35**, L14813, doi:10.1029/2008GL034374.

——, F. D. Marks Jr., M. T. Montgomery, and S. Lorsolo, 2011a: An estimation of turbulent characteristics in the low-level region of intense Hurricanes Allen (1980) and Hugo (1989). *Mon. Wea. Rev.*, **139**, 1447–1462, doi:10.1175/2010MWR3435.1.

——, R. F. Rogers, D. S. Nolan, and F. D. Marks, 2011b: On the characteristic height scales of the hurricane boundary layer. *Mon. Wea. Rev.*, **139**, 2523–2535, doi:10.1175/MWR-D-10-05017.1.

——, S. G. Gopalakrishnan, F. D. Marks, R. F. Rogers, and V. Tallapragada, 2012: A developmental framework for improving hurricane model physical parameterization using aircraft observations. *Trop. Cyclone Res. Rev.*, **1**, 419–429, doi:10.6057/2012tcrr04.01.

——, D. S. Nolan, R. F. Rogers, and V. Tallapragada, 2015: Evaluating the impact of improvements in the boundary layer parameterization on hurricane intensity and structure forecasts in HWRF. *Mon. Wea. Rev.*, **143**, 3136–3155, doi:10.1175/MWR-D-14-00339.1.

Zhu, P., K. Menelaou, and Z.-D. Zhu, 2014: Impact of subgrid-scale vertical turbulent mixing on eyewall asymmetric structures and mesovorticies of hurricanes. *Quart. J. Roy. Meteor. Soc.*, **140**, 416–438, doi:10.1002/qj.2147.